Mechanical property alterations across the cerebral cortex due to Alzheimer's disease

BRAIN COMMUNICATIONS

Mechanical property alterations across the cerebral cortex due to Alzheimer's disease

Lucy V. Hiscox,[1,2] Curtis L. Johnson,[2] Matthew D. J. McGarry,[3] Helen Marshall,[4] Craig W. Ritchie,[5] Edwin J. R. van Beek ,[4] Neil Roberts[4] and John M. Starr[1,*]

*Deceased December 2018.

Alzheimer's disease is a personally devastating neurodegenerative disorder and a major public health concern. There is an urgent need for medical imaging techniques that better characterize the early stages and monitor the progression of the disease. Magnetic resonance elastography (MRE) is a relatively new and highly sensitive MRI technique that can non-invasively assess tissue microstructural integrity via measurement of brain viscoelastic mechanical properties. For the first time, we use high-resolution MRE methods to conduct a voxel-wise MRE investigation and state-of-the-art *post hoc* region of interest analysis of the viscoelastic properties of the cerebral cortex in patients with Alzheimer's disease ($N = 11$) compared with cognitively healthy older adults ($N = 12$). We replicated previous findings that have reported significant volume and stiffness reductions at the whole-brain level. Significant reductions in volume were also observed in Alzheimer's disease when white matter, cortical grey matter and subcortical grey matter compartments were considered separately; lower stiffness was also observed in white matter and cortical grey matter, but not in subcortical grey matter. Voxel-based morphometry of both cortical and subcortical grey matter revealed localized reductions in volume due to Alzheimer's disease in the hippocampus, fusiform, middle, superior temporal gyri and precuneus. Similarly, voxel-based MRE identified lower stiffness in the middle and superior temporal gyri and precuneus, although the spatial distribution of these effects was not identical to the pattern of volume reduction. Notably, MRE additionally identified stiffness deficits in the operculum and precentral gyrus located within the frontal lobe; regions that did not undergo volume loss identified through voxel-based morphometry. Voxel-based-morphometry and voxel-based MRE results were confirmed by a complementary *post hoc* region-of-interest approach in native space where the viscoelastic changes remained significant even after statistically controlling for regional volumes. The pattern of reduction in cortical stiffness observed in Alzheimer's disease patients raises the possibility that MRE may provide unique insights regarding the neural mechanisms which underlie the development and progression of the disease. The measured mechanical property changes that we have observed warrant further exploration to investigate the diagnostic usefulness of MRE in cases of Alzheimer's disease and other dementias.

1 Alzheimer Scotland Dementia Research Centre, University of Edinburgh, Edinburgh EH8 9JZ, UK
2 Department of Biomedical Engineering, University of Delaware, Newark, DE 19713, USA
3 Thayer School of Engineering, Dartmouth College, Hanover, NH 03755, USA
4 Edinburgh Imaging Facility, School of Clinical Sciences, The Queen's Medical Research Institute (QMRI), University of Edinburgh, Edinburgh EH16 4TJ, UK
5 Centre for Dementia Prevention at Centre for Clinical Brain Sciences, University of Edinburgh, Edinburgh EH16 4UX, UK

Correspondence to: Lucy V. Hiscox, PhD
University of Delaware STAR Campus
Department of Biomedical Engineering
540 S College Ave, Newark, DE 19713, USA
E-mail: lvhiscox@udel.edu

Keywords: Alzheimer's disease; dementia; magnetic resonance elastography; voxel-based morphometry; viscoelasticity

Received May 13, 2019. Revised November 25, 2019. Accepted December 6, 2019. Advance Access publication December 17, 2019

Abbreviations: CAT12 = computational anatomy toolbox; CE = cerebrum; CGM = cortical grey matter; eTIV = estimated total intracranial volume; GM = grey matter; MRE = magnetic resonance elastography; NLI = non-linear inversion; OA = older adults; SGM = subcortical grey matter; SPR = soft prior regularization; VBM = voxel-based morphometry; VB-MRE = voxel-based magnetic resonance elastography; WM = white matter

Graphical Abstract

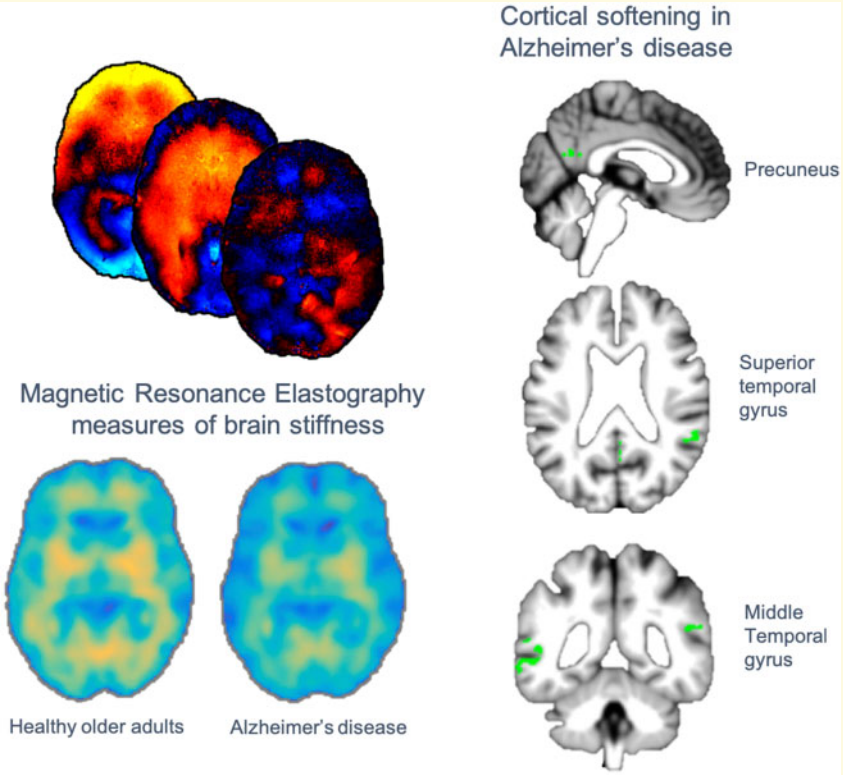

Introduction

Alzheimer's disease (AD) is the most common progressive neurodegenerative brain disorder that causes dementia. Individuals diagnosed with AD experience increasing cognitive decline, most commonly involving memory, which ultimately severely affects individuals in activities of daily living. Due to an ageing population and increasing prevalence with advancing age, AD is expected to impact millions more people worldwide and as such also represents an urgent public health concern (Alzheimer's Association, 2018). While evidence suggests that AD neuropathology begins decades before the emergence of clinical symptoms (Gonneaud *et al.*, 2017), AD can still only be detected clinically in its end phase, thus improved methods for disease detection and monitoring progression may ultimately lead to progress in preventative medicine (Ritchie *et al.*, 2015).

AD is characterized by distinct and recognizable neuropathological processes that include primary cardinal lesions of extracellular amyloid-beta plaques and neurons containing neurofibrillary tangles (Canter *et al.*, 2016), each of which possesses a characteristic distribution. Plaques are found throughout the cortical mantle, whereas tangles are primarily located in limbic and association cortices (Braak and Braak, 1991). Vascular damage from extensive plaque deposition, and eventual neuronal and synaptic loss within the cerebral cortex are other major hallmarks of AD that may be observed *in vivo* through the use of several biomarkers (Rodriguez-Arellano *et al.*, 2016). According to the dynamic amyloid cascade model (Hardy and Higgins, 1992), AD biomarkers evolve in a sequential but temporally overlapping manner (Jack *et al.*, 2010), with it being suggested that amyloid is a causative agent that acts upstream to eventual downstream neurodegeneration. This linear progression, however, remains mostly theoretical with empirical data currently being collected. Nevertheless, characterization of the structural degeneration in AD has been important for understanding AD pathology and the association with clinical outcomes.

Among the core imaging biomarkers for AD, along with amyloid PET, is measurement of cerebral atrophy measured with MRI (Jack *et al.*, 2011). The characteristic

traits estimated from structural MRI include reduced grey matter (GM) volumes, especially in the medial temporal lobe (Frisoni *et al.*, 2010). Indeed, reduced hippocampal volume, a medial temporal lobe structure implicated in memory formation, has been deemed an appropriate selection marker for clinical trials of people in the early stages of AD (European Medicines Agency, 2011). MRI volumetry, however, is only sensitive to AD relatively late in the course of the disease (Jack *et al.*, 2011), when the neurodegeneration it represents is perhaps irreversible due to such wide-spread neuronal loss. Imaging measures that more sensitively assess brain microstructural integrity can support disease detection, disease monitoring and the development of new targets for pharmaceutical intervention.

Biophysical metrics that may provide additional information regarding AD pathology are the mechanical properties of brain tissue, which act as proxies for changes in underlying microstructural tissue integrity (Sack *et al.*, 2013). Magnetic resonance elastography (MRE) is an emerging non-invasive imaging technique that can measure such viscoelastic tissue properties *in vivo* (Muthupillai *et al.*, 1995) and has been used by several groups to investigate a wide range of neurological disorders [for reviews see Hiscox *et al.* (2016) and Murphy *et al.* (2019)]. MRE is an imaging technique with high sensitivity to changes in the microstructural properties of tissues which can cause tissue stiffness to vary over a very wide dynamic range in health and disease (Mariappan *et al.*, 2010). MRE combines mechanical wave propagation and MRI phase-contrast imaging to record harmonic displacements through soft tissue, which are then 'inverted' to create maps of the underlying viscoelasticity. Viscoelasticity measurements may reflect several different characteristics of underlying neural tissue microstructure including different cell types (Lu *et al.*, 2006), their density (Freimann *et al.*, 2013; Klein *et al.*, 2014), degree of myelin content (Schregel *et al.*, 2012; Weickenmeier *et al.*, 2016, 2017), as well as several other factors including inflammation (Riek *et al.*, 2012) and oedema (Bigot *et al.*, 2018; Menal *et al.*, 2018).

An initial MRE study on AD revealed a 7% decrease in global brain stiffness, comprising both grey and white matter (WM), in biomarker-confirmed AD patients compared with age-matched controls (Murphy *et al.*, 2011). The decrease in stiffness was unrelated to amyloid accumulation and instead was suggested to reflect several microstructural events that impact normal cytoarchitectural integrity, through, for example, degradation of the extracellular matrix following amyloid deposition, tau hyperphosphorylation, or loss of interconnecting synaptic networks (Murphy *et al.*, 2011). The same group subsequently reported that the stiffness reduction in AD mainly occurred in the frontal, parietal and temporal lobes, in accordance with the known topography of AD pathology (Murphy *et al.*, 2016); this meta-region of interest analysis outperformed all other regions for discriminating between AD patients and healthy control participants. Softening of the frontal, parietal and temporal region also appears to be specific to dementia of the Alzheimer's type: unique variations among regional brain stiffness were reported between common dementia subtypes that included AD, dementia with Lewy bodies, frontotemporal dementia and normal pressure hydrocephalus (ElSheikh *et al.*, 2017). These findings are supported by studies using transgenic animal models that have demonstrated that MRE is sensitive to AD pathophysiology, with reduced brain stiffness being found in both APP-PS1 (Murphy *et al.*, 2012) and APP23 (Munder *et al.*, 2018) type mice.

Furthermore, it was recently reported that viscoelasticity of the hippocampus was altered in AD and MRE could improve the diagnostic accuracy of MRI exams (Gerischer *et al.*, 2018). Notably, MRE has also been used to identify structure–function relationships in healthy participants between hippocampal viscoelasticity and memory (Schwarb *et al.*, 2016; Hiscox *et al.*, 2018*b*) and the viscoelasticity of the orbitofrontal cortex and fluid intelligence (Johnson *et al.*, 2018), whereas volumetric measures were not reported to correlate with function. These studies highlight how mechanical property measures are sensitive to individual differences in cognition and suggest that MRE may enhance the information obtained from volumetric MRI.

In this current cross-sectional exploratory study, we will utilize structural MRI and high-resolution MRE to study volumetric and viscoelastic properties of the brain in both AD patients and healthy older adults (OA). First, we will perform an analysis of global regions of interest (ROIs) such as the global cerebrum (CE), WM, cortical grey matter (CGM) and subcortical grey matter (SGM) to establish whether our results replicate previous report (Murphy *et al.*, 2011, 2016; Gerischer *et al.*, 2018). As such, we predict that AD patients will exhibit reduced brain volumes and stiffness compared with OA. Second, we will perform an exploratory, data-driven, voxel-wise analysis to potentially identify specific GM regions that display volumetric and/or viscoelastic alterations in participants with AD. A data-driven analysis is compelled by the collected data, rather than by a specific *a priori* hypothesis and is used in lieu of an ROI-based approach to potentially reveal alterations in mechanical properties that may not have been previously reported or hypothesized. As AD is recognized as primarily a disease of the cortex, we constrain our voxel-wise analysis to GM (cortical and subcortical) to increase statistical power in this preliminary investigation. Third, we will perform a complementary *post hoc* ROI analysis in native space of the volume and viscoelasticity of regions identified by the voxel-wise analyses. For MRE measures, we will statistically control for the volume of each ROI to investigate whether MRE results remain the same after accounting for ROI volume size.

Materials and methods

Participants

Demographic information for all participants is presented in Table 1. Patients with AD ($N = 12$; 7 F/5M; mean age 77.2) were recruited from sources including the Join Dementia Research (JDR) database (see Acknowledgements section), the memory clinic at the Weston General Hospital, Edinburgh and the Centre for Dementia Prevention, University of Edinburgh. All patients had been diagnosed with AD before entering the study and met the NICE guidelines for probable dementia due to AD. One MRE dataset was excluded (see MRE analysis with non-linear inversion); as a result, the total number of AD participants included in the MRE portion of the analyses was $N = 11$ (7 F/4M; mean age 76.8). All healthy OA control participants ($N = 12$; 6 F/6M; mean age 69.4) were recruited from the JDR database and have been studied using identical MRE data acquisition and analysis protocols and reported on previously (Hiscox *et al.*, 2018*a*, *b*). All OA participants had no subjective memory complaints and scored at least 26 out of 30 on the MoCA which suggests normal cognitive functioning (Nasreddine *et al.*, 2005; mean = 28.1; range = 26–30). There was no difference between groups due to sex; however, the groups differed in age [t (22) $= 4.5$, $P < 0.001$], with AD participants being significantly older than OA participants, and scores on the MoCA [t (22) $= 7.6$, $P < 0.001$], as expected. All participants were predominantly right-handed as determined by the Edinburgh Handedness Inventory (EHI), except for one left-handed AD patient. Exclusion criteria for both groups included: (i) history or current diagnosis of a psychiatric disorder; (ii) history of major head injury; (iii) no psychoactive medications; and (iv) contraindications for undergoing brain MRI. The study was approved by the National Health Service Lothian Research Ethics Committee (REC) and all study participants gave written, informed consent of their willingness to participate prior to the examination. As all patients were in the mild-to-moderate stages of AD, they were deemed clinically capable of providing their own informed consent but attended the visit with a designated study partner.

Imaging acquisition

Brain imaging data were collected using a Siemens 3T Verio whole-body MRI scanner with a 12-channel head receive only coil (Siemens Healthineers, Erlangen, Germany). The imaging protocol included a high-resolution T_1-weighted anatomical scan using an MPRAGE pulse sequence (magnetization-prepared rapid gradient echo; TR = 2300 ms; TE = 2.98; flip angle = 9 degrees; voxel size = 1 × 1 × 1 mm^3), and a fluid-attenuated inversion recovery (FLAIR) scan (TR = 10 000 ms; TE = 97; flip angle = 150 degrees; voxel size = 0.94 × 0.94 × 5 mm^3). The MRE portion of the experiment involves gently vibrating the head to generate shear waves that propagate through the brain creating tissue displacements of the order of microns. A commercially available pneumatic actuator system was used for this purpose (Resoundant^{TM}, Rochester, MN, USA). Vibrations were generated at 50 Hz frequency (20% amplitude) and delivered to the head through a soft passive pillow driver. The MRE acquisition used a 3D multislab, multishot spiral sequence synchronized to these vibrations to capture high-resolution displacement data (Johnson *et al.*, 2014). Imaging parameters included: 1800/75 ms repetition/echo times; 240 mm square field-of-view; 150 × 150 imaging matrix; and sixty 1.6-mm thick contiguous slices. The resulting imaging volume had a 1.6 × 1.6 × 1.6 mm^3 voxel size with 96 mm of coverage in the slab direction, which was aligned approximately to the anterior commissure–posterior commissure (AC-PC) line. The resulting tissue deformation was encoded using motion-sensitive gradients embedded in the MRE sequence, which was repeated to capture motion along three separate axes, with opposite gradient polarities, and through four phase offsets to observe wave propagation in time. The total MRE acquisition time was approximately 12 min.

Table 1 Demographic data

	OA	AD	
		Volumetry	MRE
Number	12	12	11
Sex	6F/6M	7F/5M	7F/4M
Age	69.4 (66–73)	77.2 (70–87)	76.8 (70–87)
MoCA	28.1 (26–30)	18.3 (10–27)	18.4 (10–27)
EHI	+0.86 (+0.3–1)	+0.84 (−0.9–1)	+0.84 (−0.9–1)
eTIV (cm^3)	1432 + 136	1410 + 114	1408 + 119

Data are mean values with range in parenthesis. AD = patients with Alzheimer's disease; OA = healthy older adult control; MoCA = Montreal cognitive assessment; EHI = Edinburgh handedness inventory; eTIV = estimated total intracranial volume.

MRE analysis with non-linear inversion

Non-linear inversion (NLI) was used to recover maps of complex-valued viscoelastic shear modulus ($G^* = G' + iG''$) that reflect both elastic energy storage and viscous energy attenuation. NLI techniques use finite-element methods to invoke a computational model of the mechanical motion of heterogeneous tissue, and iteratively estimate a set of mechanical property parameters that best reproduces the measured displacements (Van Houten *et al.*, 1999; McGarry *et al.*, 2012). Displacement data in MRE native space were supplied to NLI which returns property maps across the entire brain as defined by a binary mask. The resolution of the mechanical property and displacement meshes was set to the same resolution as the displacement data (1.6 mm), which is a standardized procedure used in several previous brain MRE

studies (Schwarb *et al.*, 2016; Johnson *et al.*, 2018). As with our previous work, we reformulated the complex shear modulus G^* to determine the shear stiffness μ, and damping ratio, ξ. Shear stiffness, defined as $\mu = 2|G^*|^2/(G'+|G^*|)$, describes the resistance of a material to a harmonic shear stress at the given actuation frequency, and is related to the square of the wave speed in a viscoelastic material with density of 1000 kg/m. Generally, the stiffness parameter is related to the strength of the composition of the tissue network (Sack *et al.*, 2013), but depending on the type of disease may reflect different biological processes. Damping ratio, ξ, is a dimensionless quantity describing the relative attenuation level in the material, defined as $\xi = G''/2G'$ (McGarry and Van Houten, 2008), or the relative viscous-to-elastic behaviour of the tissue, and is often considered to reflect tissue organization at the microscale. The exact neurobiological correlates of the damping ratio, however, are currently less well understood (Johnson *et al.*, 2018). Finally, we removed voxels containing over 50% cerebrospinal fluid from both MRE parameter maps through the co-registration of cerebrospinal fluid partial intensity images generated through Statistical Parametric Mapping software (SPM12 v7487, University College London, London, UK). One MRE dataset (AD patient) did not pass the octahedral shear strain-based signal to noise ratio threshold for sufficiently high-quality displacement data for stable inversion (>3; McGarry *et al.*, 2011), and as a result, as mentioned above, the total number of participants included in the MRE portion of these analyses was 23 (12 OA controls; 11 AD patients).

Analysis 1: Global analyses

Initial analyses assessed volumetric and viscoelastic differences in the brain between AD patients and OA participants for the bilateral CE, WM, CGM, and SGM. Volumes were generated from the FreeSurfer software pipeline (v6.0; Fischl *et al.*, 2002) using the default settings, with values used from BrainSegNotVent (i.e. segmentation volume without the ventricles), total cerebral WM volume, total CGM volume and SGM volume. The estimated total intracranial volume (eTIV) was calculated using SPM as Freesurfer eTIV has been discovered to be biased by the size of the total brain volume (Klasson *et al.*,); eTIV was used to normalize each region of interest so as to account for individual differences in head size using an adjustment formula based on the analysis of covariance (ANCOVA) approach (Raz *et al.*, 2005). Mean cortical thickness measures were also obtained from SPM for each participant. These same ROIs were then used as subject-specific MRE masks. The SGM template was custom-made and contained the nucleus accumbens, amygdala, caudate, hippocampus, pallidum, putamen and thalamus, and the global ROI was a combined WM, CGM and SGM mask. Each mask was then co-registered to the MRE magnitude images using FMRIB's Linear Image Registration Tool (FLIRT) within the FMRIB Software Library (FSL) using the inverse transform of MRE-to-T1 (Jenkinson *et al.*, 2012). As a result, μ and ξ values for each ROI were obtained in MRE native space for each individual. Example MRE μ images are shown in Fig. 1A and B. A one-way univariate general linear model (ANCOVA) was used to examine the effect of AD on each global cerebral ROI as compared with OA. As age has previously been shown to affect the underlying viscoelastic properties of different brain regions (Arani *et al.*, 2015; Hiscox *et al.*, 2018*a*), age (in years) was included as a covariate. Separate ANCOVAs were conducted for each ROI and for volume, μ and ξ separately.

Analysis 2: Voxel-wise analyses

An exploratory, data-driven approach using voxel-wise statistics was performed to investigate GM differences in brain tissue volume and mechanical properties between AD and OA participants. Voxel-based morphometry (VBM) and voxel-based MRE (VB-MRE) analyses were conducted by using SPM executed through the computational anatomy toolbox (CAT12) within MATLAB R2019a (MathWorks, Natick, MA, USA). Due to the importance of being explicit about the assumptions underlying key methodological choices made in VBM analyses (Peelle *et al.*, 2012), the pipeline is thoroughly described in the Supplementary material. In brief, T_1-weighted images were corrected for WM hypo-intensities by processing the acquired FLAIR images through the lesion growth algorithm (Schmidt *et al.*, 2012) as implemented in the LST toolbox version 2.0.15 (www.statistical modelling.de/lst.html). The corrected T_1-weighted images were then segmented into GM, WM and cerebrospinal fluid using the six-class default tissue probability map available in SPM. During segmentation, the images were simultaneously subjected to an affine anatomical standardization to the Montreal Neurological Institute (MNI) 152 IX I155 template using 'DARTEL export'. The affine GM and WM non-modulated volumes were then processed through DARTEL, the fast-diffeomorphic image registration algorithm (Ashburner, 2007) to provide a more accurate spatial normalization optimized for the population under study. Through this procedure, flow fields that describe the transformation from each native space image to the resulting study-specific template are generated. For VBM, the resulting flow fields were applied to the affine GM images and modulated to preserve the total amount of signal from each region; areas that expanded during warping are correspondingly reduced in intensity. Images were then smoothed with an 8 mm FMHM Gaussian filter and kept at the default isotropic resolution of 1.5 mm. For VB-MRE, a rigid-body registration was used to estimate the transformation between the MRE magnitude image and the corresponding subject-specific T_1-weighted image. This rigid-body transformation was applied to the NIFTI orientation matrix only, and then the

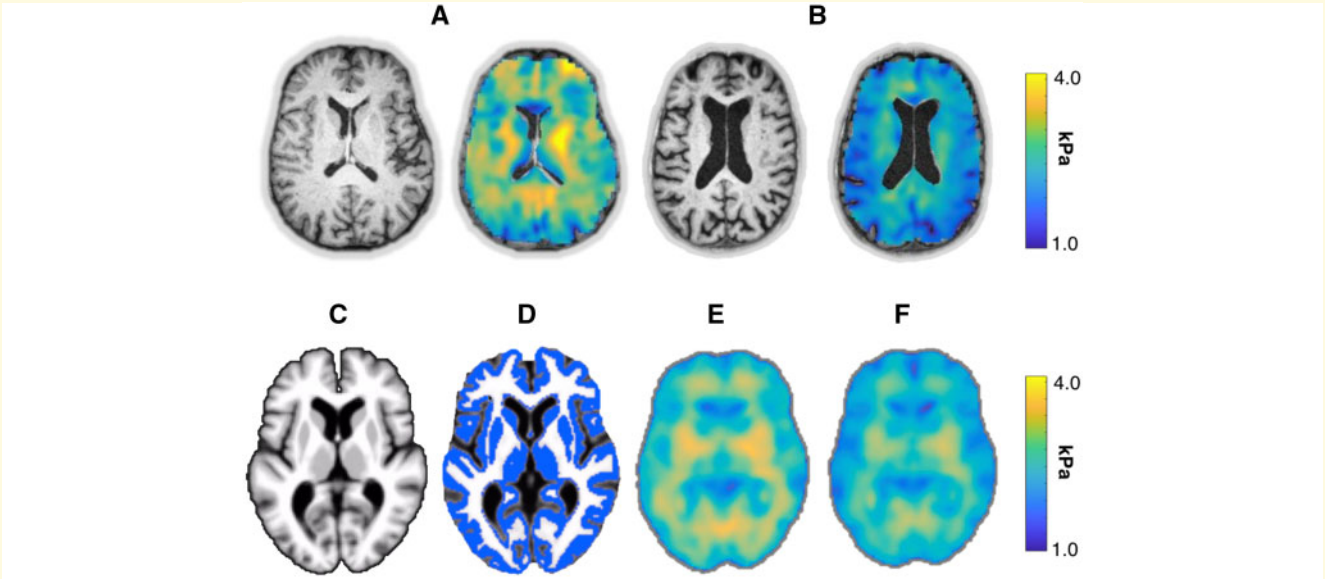

Figure 1 Example T_1-weighted and MRE shear stiffness, μ, images. (**A**) The structural anatomical image and stiffness map for a healthy 68-year-old female control (OA), and (**B**) the same information for a 71-year-old female with Alzheimer's disease. (**C**) The study-specific template in MNI space that was generated through DARTEL, and (**D**) the grey matter mask used for VBM and VBM-MRE. The normalized mean stiffness maps are provided for OA andAD participants in **E** and **F**, respectively.

same flow fields to the DARTEL template were applied. MRE images were not modulated (i.e. set to *preserve concentrations*) to preserve the intensities of the original images, and a Gaussian filter width of 2 mm was applied as MRE images are naturally smooth due to the solution of the MRE inverse problem. For the VBM analysis only, eTIV was included as a nuisance variable in the ANCOVA model; eTIV is not expected to effect brain viscoelasticity. For both analyses, age and sex were included as covariates centred at the mean, and with no centring, respectively. An explicit GM mask was applied which had been generated from the mean T_1 DARTEL template, segmented, thresholded at 100% and binarized, as shown in Fig. 1C and D. Two-sample *t*-tests were performed on the spatially normalized MRI volumes and MRE μ and ξ images between OA and AD. We specified the *t*-contrast (−1, 1; AD < OA) and set the statistical threshold at $P < 0.001$, uncorrected for multiple comparisons. Only clusters with a minimum of 20 voxels are reported. The anatomical labels of the MNI coordinates were defined using automated anatomical labelling (Tzourio-Mazoyer *et al.*, 2002), which was implemented with the Wake Forest University (WFU) Pick Atlas software (v3.03) (Maldjian *et al.*, 2003). Mean normalized maps of OA and AD participants are provided in Fig. 1E and F, respectively.

Analysis 3: Post hoc *ROI analyses*

By using the regions identified as differing in volume or MRE measures between AD and OA groups (Analysis 2), we performed *post hoc* ROI analyses. In particular, volumetric parcellations of GM were obtained from FreeSurfer, normalized according to eTIV, and used as dependent variables. For regions identified by the VB-MRE analysis, ROI masks for each subject were extracted from the FreeSurfer Desikan-Killiany parcellation scheme (Desikan *et al.*, 2006), and converted into masks in MRE native space using FLIRT in FSL (Jenkinson *et al.*, 2012). After registration, cortical masks were thresholded at 50% and input into the NLI algorithm as *a priori* spatial information as part of the soft prior regularization (SPR) routine (McGarry *et al.*, 2013). SPR reduces heterogeneity in an ROI and has been shown to improve sensitivity measures in MRE studies of subcortical GM (Johnson *et al.*, 2016) and has recently been introduced for MRE of cortical structures (Johnson *et al.*, 2018; Schwarb *et al.*, 2019). An SPR weighting of $\alpha = 10^{-10}$ was chosen to minimize influence from surrounding tissues while still allowing for individual differences in regional properties to be preserved. Results for various regularization weightings ($\alpha = 10^{-10}$, $\alpha = 10^{-11}$, $\alpha = 10^{-12}$) as well as those acquired without SPR are provided in Supplementary Table 1. We performed a one-way univariate ANCOVA to assess the effect of AD on each ROI. Analyses for volume and for MRE metrics were performed separately and included age as a covariate. A secondary analysis added regional volume as a covariate. All statistical analyses were performed with IBM SPSS Statistics for Mac, version 25.0.0 (IBM Corp., Armonk, NY, USA).

Statistical analyses

Statistical analyses for each performed analysis are described above. In brief, VBM and VB-MRE analyses (Analysis 2) were conducted by using SPM executed

through CAT12. For both the global analysis (Analysis 1) and *post hoc* ROI analysis (Analysis 3), one-way univariate general linear models (ANCOVA) were used to examine the effect of AD on each ROI as compared with OA using SPSS.

Data availability

The data that support the findings of this study are available from the corresponding author, upon reasonable request.

Results

In Analysis 1, we report the results from the global volumetric and MRE analyses. Analysis 2 contains the exploratory voxel-wise results for both VBM and voxel-based magnetic resonance elastography (VB-MRE), and Analysis 3 uses a *post hoc* ROI approach to further investigate the results from the voxel-wise investigations.

Analysis 1: Global analyses

The average octahedral shear strain-based signal to noise ratio of brain MRE data was 6.02 ± 1.67 and 6.20 ± 1.17 for the OA and AD cohorts [$t\ (21) = -0.30$, $P = 0.77$], respectively, indicating high-quality whole-brain displacement data. Descriptive statistics regarding *P*-values, and effect sizes for MRI volumetry and MRE shear stiffness, μ, and MRE damping ratio, ξ, values for each global ROI [i.e. CE, WM, CGM and SGM], for both AD and OA participants are presented in Table 2. One-way univariate general linear models (ANCOVAs) were performed to examine the effect of disease on each parameter for each global compartment using age (years) as a covariate; each analysis was performed separately. Both the mean values (M) and mean age-adjusted values (M_{adj}) are presented.

Volume

There was a statistically significant effect of AD on CE volume ($P = 0.001$), indicating AD patients had lower CE volumes ($M_{adj} = 989\,cm^3$) compared with OA ($M_{adj} = 1092\,cm^3$). The AD group had, on average, a 10% reduction in the size of CE. Similar effects for WM, CGM and SGM volumes were found ($P = 0.013$, $P = 0.001$ and $P = 0.015$, respectively). On average, the AD group had deficits of 13%, 9% and 8% for WM, CGM and SGM volumes, respectively. We found no significant difference between groups with regards to mean cortical thickness measurements ($P = 0.073$).

Shear stiffness

AD had a significant effect on CE μ ($P = 0.004$), indicating AD patients had lower overall brain stiffness ($M_{adj} = 2.25\,kPa$) compared with OA participants ($M_{adj} = 2.50\,kPa$). The AD group had, on average, 11% lower CE μ. Similar effects for WM and CGM μ were found. Compared with OA participants, AD patients had lower WM μ (2.38 kPa vs. 2.61 kPa; $P = 0.022$) and lower CGM μ (2.02 kPa vs. 2.32 kPa; $P < 0.001$). On average, the AD group had 9% lower WM μ and 14% lower CGM μ. In contrast, no difference between groups was observed for SGM ($P = 0.27$). These comparisons are presented in Fig. 2.

Damping ratio

There was no significant effect of AD on CE ξ ($P = 0.51$), indicating no discernible differences in CE ξ between AD ($M_{adj} = 0.262$) and OA ($M_{adj} = 0.256$). Similarly, we found no significant effect of AD on WM ξ ($P = 0.81$), CGM ξ ($P = 0.40$) or SGM ξ ($P = 0.08$), as shown in Fig. 2.

Analysis 2: VBM and VB-MRE analyses

GM volume

Using a data-driven voxel-wise analysis, we found that, compared with OA, the AD group had significantly lower GM volume in the fusiform gyrus (bilaterally), superior temporal gyrus (bilaterally), left middle temporal gyrus, right precuneus and right hippocampus. Peak MNI coordinates, *t*-scores and cluster sizes are provided in Table 3a. Significant differences in clusters of voxels between groups are illustrated in Fig. 3A.

GM viscoelasticity

Compared with OA, AD participants had significantly lower GM stiffness, μ, in the superior temporal gyrus (bilaterally), left middle temporal gyrus, the right frontal operculum/precentral gyrus and the right precuneus. Peak MNI coordinates, *t*-scores and cluster sizes are presented in Table 3b. Clusters of voxels which represent significant differences in GM viscoelasticity between groups are displayed in Fig. 3B. We additionally performed an MRE voxel-wise analysis on damping ratio, ξ; consistent with our global analysis, we found no significant clusters between groups and thus ξ was not considered further. The *post hoc* ROI analysis results for ξ are presented in Supplementary Table 2.

Analysis 3: Post hoc ROI analyses

Results from Analysis 2 subsequently informed our choice of ROIs to be used in our *post hoc* ROI analyses. All ROIs identified by either VBM or VB-MRE were included, thus resulting in the analysis of seven cortical parcellations as well as the hippocampus. One-way ANOVAs were performed separately to assess the effects of AD on both volume and μ. A secondary analysis included controlling for regional volumes, as shown in Table 4.

Table 2 Results of the voxel-wise VBM and VB-MRE analyses

	OA	AD	|F|	*P*-value	partial η^2
Volume					
Cerebrum					
$M \pm SD$	1102 ± 35	979 ± 60			
$M_{adj} \pm SE$	1092 ± 17	989 ± 17	13.77	**0.001*****	0.40
White Matter					
$M \pm SD$	455 ± 24	400 ± 42			
$M_{adj} \pm SE$	455 ± 12	400 ± 12	7.39	**0.0132***	0.26
Cortical grey matter					
$M \pm SD$	465 ± 18	406 ± 25			
$M_{adj} \pm SE$	456 ± 7	415 ± 7	13.49	**0.001*****	0.39
Subcortical grey matter					
$M \pm SD$	52.8 ± 3.1	48.2 ± 2.2			
$M_{adj} \pm SE$	52.5 ± 0.9	48.5 ± 0.9	7.05	**0.0153***	0.25
Cortical thickness (mm^3)					
$M \pm SD$	2.56 ± 0.11	2.39 ± 0.09			
$M_{adj} \pm SE$	2.52 ± 0.03	2.42 ± 0.03	3.58	0.073	0.15
Shear stiffness, μ					
Cerebrum					
$M \pm SD$	2.52 ± 0.13	2.23 ± 0.15			
$M_{adj} \pm SE$	2.50 ± 0.05	2.25 ± 0.05	10.57	**0.004****	0.35
White Matter					
$M \pm SD$	2.65 ± 0.14	2.34 ± 0.19			
$M_{adj} \pm SE$	2.61 ± 0.06	2.38 ± 0.06	6.30	**0.0224***	0.24
Cerebral cortex					
$M \pm SD$	2.33 ± 0.13	2.02 ± 0.12			
$M_{adj} \pm SE$	2.32 ± 0.04	2.02 ± 0.05	17.55	**0.001*****	0.47
Subcortical grey matter					
$M \pm SD$	2.73 ± 0.23	2.55 ± 0.19			
$M_{adj} \pm SE$	2.71 ± 0.08	2.57 ± 0.08	1.31	0.275	0.06
Damping ratio, ξ					
Cerebrum					
$M \pm SD$	0.257 ± 0.015	0.262 ± 0.014			
$M_{adj} \pm SE$	0.256 ± 0.005	0.262 ± 0.005	0.45	0.517	0.02
White Matter					
$M \pm SD$	0.257 ± 0.015	0.262 ± 0.011			
$M_{adj} \pm SE$	0.258 ± 0.005	0.260 ± 0.005	0.06	0.814	0.003
Cerebral cortex					
$M \pm SD$	0.266 ± 0.020	0.270 ± 0.018			
$M_{adj} \pm SE$	0.264 ± 0.007	0.273 ± 0.007	0.76	0.406	0.04
Subcortical grey matter					
$M \pm SD$	0.223 ± 0.014	0.234 ± 0.019			
$M_{adj} \pm SE$	0.220 ± 0.006	0.237 ± 0.006	3.42	0.079	0.15

Volumes provided in units of cm^3, shear stiffness, μ, in kilopascals (kPa) and damping ratio, ξ, is dimensionless. M_{adj} values are age-adjusted results ± standard error. OA = healthy older adult controls; AD = patients with Alzheimer's disease.
*** denotes $P < 0.001$, ** denotes $P < 0.01$ and * denotes $P < 0.05$ significance levels.

GM volume

Controlling for participant age, there was a significant effect of AD on the volume of the hippocampus ($P = 0.008$), fusiform gyrus ($P = 0.010$), inferior temporal gyrus ($P = 0.009$), middle temporal gyrus ($P = 0.029$) and precuneus ($P = 0.007$). No significant effect of AD was found on the volume of the superior temporal gyrus ($P = 0.070$), operculum ($P = 0.161$) or precentral gyrus ($P = 0.413$).

GM viscoelasticity

A significant effect of AD on shear stiffness, μ, was found for the fusiform gyrus ($P = 0.005$), inferior temporal gyrus ($P = 0.005$), middle temporal gyrus ($P = 0.001$), superior temporal gyrus ($P = 0.001$), operculum ($P = 0.009$), precentral gyrus ($P = 0.028$) and precuneus ($P = 0.002$). In contrast, AD did not significantly affect hippocampal μ ($P = 0.71$). Next, we performed a one-way univariate ANCOVA to correct μ results for volume size, with each ROI analysis performed separately. All regions remained significantly affected by AD after additionally controlling for ROI volume size except for fusiform gyrus ($P = 0.15$) and inferior temporal gyrus ($P = 0.06$). A summary of the relationships found among ROI, μ and volume size are illustrated in the correlation matrix provided in Supplementary Fig. 1.

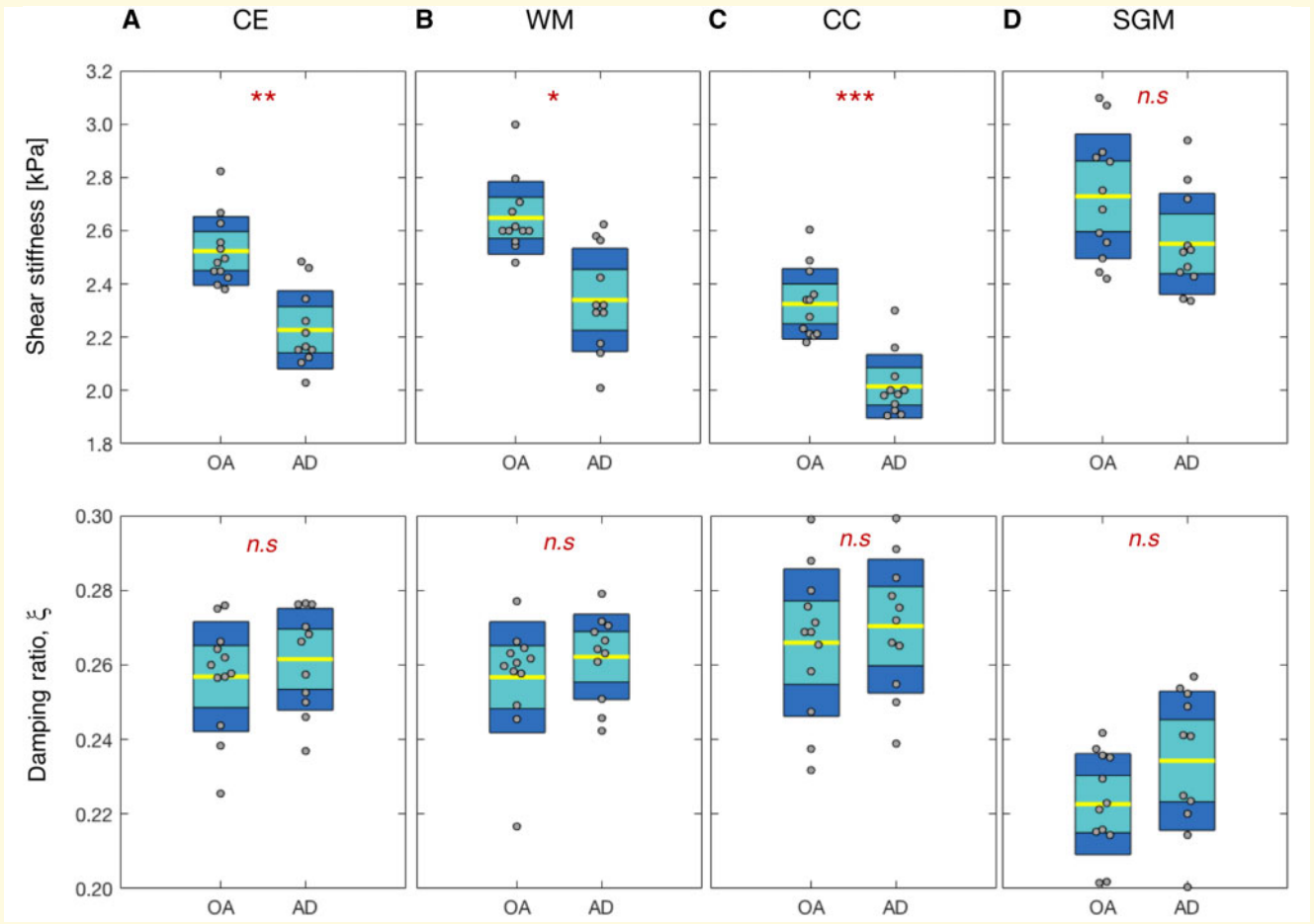

Figure 2 Boxplots illustrating μ (top row) and ξ (bottom row) values for OA and AD groups for each global ROI (A=cerebrum; B=white matter; C=cortical grey matter; D=subcortical grey matter). The yellow line represents the group mean, the green area is the 95% confidence interval and the area in blue is ±1 standard deviation. Jittered data (circles) are individual values.

Discussion

This work builds on previous studies that have analysed the mechanical properties of the brain *in vivo* in patients with AD. In this study, we have taken advantage of high-resolution MRE methods in combination with an exploratory data-driven approach to reveal new insights into microstructural integrity observed across the cerebral cortex due to AD.

Overall, we report a global reduction in both brain volume and stiffness in patients with AD compared with cognitively healthy OA. Volume reductions in AD were reported for the global brain and for all individual compartments of the whole brain, namely WM, CGM and SGM, whereas no difference was observed between groups for measures of mean cortical thickness. Lower stiffness was also observed for the global brain and WM and was particularly evident for GM of the cerebral cortex. A subsequent exploratory GM voxel-wise analysis revealed that volume reductions were largely localized to the hippocampus and the cortex of the temporal lobe including the fusiform, middle and superior temporal gyri. Similarly, MRE revealed lower stiffness across the middle and superior temporal gyri as well as the operculum and precentral gyrus. Also, both the VBM and VB-MRE analyses revealed reduced volumes and stiffness of the precuneus. However, while similar neuro-anatomical regions were identified in the majority of the results for both analyses, the spatial distribution patterns of the differences between OA and AD were not identical. A *post hoc* ROI analysis confirmed the voxel-wise results by finding the same reduced volumes and viscoelastic deficits due to AD and that the stiffness of these regions was affected by AD even after controlling for ROI volume size.

These above results complement previous MRE studies of AD which also found that AD patients have a reduction in brain stiffness compared with age-matched healthy controls. The 11% reduction in global brain stiffness that we have observed is consistent with the 7% global stiffness reduction in biomarker-confirmed probable AD reported by Murphy *et al.* (2011). Lower brain stiffness possibly reflects a number of microstructural events that

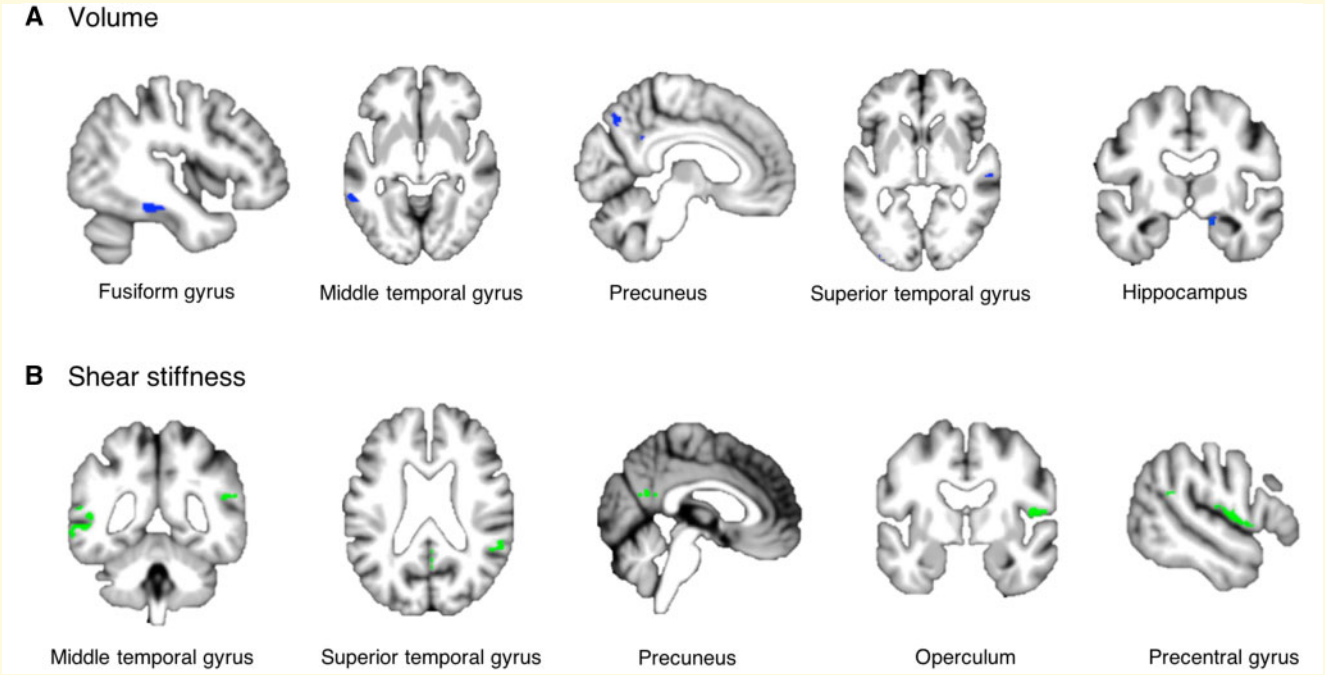

Figure 3 Voxels that show significant differences between healthy OA controls and patients with AD. Significant clusters are overlaid onto the study-specific T_1-weighted template illustrating: (**A**) regions of grey matter that show volume reductions, and (**B**) regions that are softer (i.e. possess lower shear stiffness, μ) in patients with AD compared with OA. Clusters are shown at the uncorrected $P < 0.001$ level. Images are shown in neurological convention.

Table 3 Voxel-wise analyses

MNI coordinates			Side	Lobe	Region	T-score	Size
x	y	z					
(a) Volume							
42	−35	−18	R	Temporal	Fusiform gyrus	5.14	133
−39	−25	−21	L	Temporal	Fusiform gyrus	4.62	42
−58	−47	−6	L	Temporal	Middle temporal gyrus	4.59	75
7	−68	48	R	Parietal	Precuneus	4.48	142
59	−23	−2	R	Temporal	Superior temporal gyrus	4.14	42
−55	−18	2	L	Temporal	Superior temporal gyrus	4.03	48
18	−6	−15	R	Temporal	Hippocampus	4.01	161
(b) Shear stiffness, μ							
−64	−47	−5	L	Temporal	Middle temporal gyrus	8.12	383
52	−6	10	R	Frontal	Operculum/Precentral gyrus	5.84	325
−53	−16	3	L	Temporal	Superior temporal gyrus	5.20	105
58	−44	22	R	Temporal	Superior temporal gyrus	4.55	140
3	−56	25	R	Parietal	Precuneus	4.26	27

$P < 0.001$ at voxel level (peak level), uncorrected for multiple comparisons; x, y, z: peak MNI coordinates; cluster size (in voxels); *t*-statistic represents voxel showing peak GM difference for either volume or shear stiffness, μ, between groups. Note that all clusters show significantly lower volumes and μ in AD patients (AD < OA). AD = patients with Alzheimer's disease.

characterize AD, including degradation of the extracellular matrix, loss of normal cytoskeletal architecture or altered synaptic connectivity, as suggested by Murphy *et al.* (2019), while the use of transgenic animal models have also demonstrated that MRE is sensitive to AD pathophysiology (Murphy *et al.*, 2012; Munder *et al.*, 2018). Our findings provide additional support for the interpretation that lower brain stiffness identified through MRE is sensitive to the weakening of the brain parenchyma.

Our exploratory, data-driven, voxel-wise approach to the study of the volumetric and viscoelastic properties of the brain in patients with AD has added important information in that both volume and stiffness reductions

Table 4 ***Post hoc*** **volumetric and shear stiffness, μ, values across selected ROIs**

	OA	AD	|F|	*P*-Value	partial η^2
Hippocampus					
Volume[a]	7384 ± 298	5971 ± 298	8.54	**0.008****	0.29
Stiffness[a]	2.50 ± 0.11	2.43 ± 0.12	0.14	0.715	0.01
Stiffness[b]	2.45 ± 0.11	2.48 ± 0.11	0.03	0.880	0.01
Fusiform gyrus					
Volume	19154 ± 560	16564 ± 560	8.14	**0.010***	0.28
Stiffness[a]	2.52 ± 0.06	2.22 ± 0.06	10.16	**0.005****	0.34
Stiffness[b]	2.44 ± 0.05	2.31 ± 0.06	2.22	0.153	0.10
Inferior temporal gyrus					
Volume[a]	21685 ± 718	18305 ± 718	8.42	**0.009****	0.29
Stiffness[a]	2.49 ± 0.06	2.19 ± 0.06	9.75	**0.005****	0.33
Stiffness[b]	2.45 ± 0.06	2.23 ± 0.07	3.89	0.063	0.17
Middle temporal gyrus					
Volume[a]	21363 ± 645	18915 ± 645	5.48	**0.029***	0.21
Stiffness[a]	2.53 ± 0.07	2.09 ± 0.07	15.69	**0.001*****	0.44
Stiffness[b]	2.47 ± 0.06	2.16 ± 0.07	7.96	**0.011***	0.30
Superior temporal gyrus					
Volume[a]	22814 ± 497	21272 ± 497	3.66	0.070	0.15
Stiffness[a]	2.61 ± 0.09	2.05 ± 0.09	15.71	**0.001*****	0.44
Stiffness[b]	2.55 ± 0.08	2.12 ± 0.09	9.58	**0.006****	0.34
Operculum					
Volume[a]	7986 ± 307	7264 ± 307	2.11	0.161	0.09
Stiffness[a]	2.67 ± 0.11	2.12 ± 0.12	8.47	**0.009****	0.30
Stiffness[b]	2.69 ± 0.12	2.09 ± 0.13	8.94	**0.008****	0.32
Precentral gyrus					
Volume[a]	26006 ± 763	24123 ± 763	2.32	0.413	0.10
Stiffness[a]	2.54 ± 0.15	1.95 ± 0.16	5.64	**0.028***	0.22
Stiffness[b]	2.53 ± 0.16	1.96 ± 0.17	4.57	**0.046***	0.19
Precuneus					
Volume[a]	19820 ± 625	16803 ± 625	8.87	**0.007****	0.30
Stiffness[a]	2.51 ± 0.06	2.15 ± 0.07	12.20	**0.002****	0.38
Stiffness[b]	2.54 ± 0.07	2.12 ± 0.07	11.78	**0.003****	0.38

[a]Values are age-adjusted results ± standard error.
[b]Values are adjusted for both age and regional volumes ± standard error. OA = healthy older adult controls; AD = patients with Alzheimer's disease. Values in bold indicate results that are statistically significant.
*** denotes $P < 0.001$, ** denotes $P < 0.01$ and * denotes $P < 0.05$ significance levels.

largely occur in the same neuro-anatomical regions, most of which are found across the temporal lobe. This supports the neuropathological profile of typical amnestic AD in which atrophy usually begins in the medial temporal lobes before spreading to lateral and medial parietal and temporal lobes and finally to the lateral frontal cortex, with relative sparing of the occipital lobe and sensory-motor cortex (Risacher and Saykin, 2013). The VBM results also found lower volumes of the hippocampus, which is traditionally the most studied brain region in AD (Jack *et al.*, 2008) due to its essential role in encoding and consolidating new memories (Aggleton and Brown, 1999; Eichenbaum *et al.*, 2007). Thus, the reduction in hippocampal volume observed in the present study is consistent with many previous reports (Schuff *et al.*, 2009; Halliday 2017; McRae-McKee *et al.*, 2019). We also found smaller volumes in AD within the fusiform, middle and superior temporal gyri—regions which correspond with a previously proposed 'temporal meta-ROI' to capture AD-related atrophy (Jack *et al.*, 2015). Indeed, due to prominent atrophy observed in the middle temporal gyrus, volumetric measures have been suggested for use as an AD biomarker for disease progression assessment (Spenger *et al.*, 2011). The VB-MRE results presented here complement the VBM findings by also identifying reduced cortical stiffness of the middle and superior temporal gyri. However, the spatial distribution patterns of lower stiffness from the VB-MRE analysis is not identical to the reduced volumes identified from VBM, as can be seen in Fig. 3. Importantly, our *post hoc* analysis, performed in MRE native space, confirm the exploratory voxel-wise findings. Our results are consistent with a previous MRE study of AD in which there was a significant reduction in temporal lobe stiffness in patients with AD compared with OA (Murphy *et al.*, 2016). Our higher-resolution MRE data have now localized this softening to specific regions of cortex within the temporal lobe while simultaneously demonstrating that these effects persist even after controlling for regional volumes.

Both VBM and VB-MRE analyses identified that AD patients had significantly greater atrophy and lower stiffness within the precuneus, a portion of the superior

parietal lobule. The precuneus network is an important connectivity hub in the brain and is part of the classic default-mode network (Leech and Sharp, 2014; Utevsky *et al.*, 2014) and has been reported to be among the most severely affected brain regions in AD (Migliaccio *et al.*, 2015). Resting-state fMRI studies have shown that medial parietal signal changes occur in the early stages of the disease (Agosta *et al.*, 2012), while lower GM density in the precuneus has been associated with a younger age of onset (Karas *et al.*, 2007). The observed softening of the precuneus is likely related to similar microstructural degradation underlying the loss in volume. There has been speculation that cortical amyloid retention is associated with a disrupted resting-state network of the precuneus cortex (Song *et al.*, 2015), and thus future studies may assess whether cortical softening could be directly related to disruption of these same networks.

MRE also revealed additional anatomical regions that differed between OA and AD. For example, a reduction in stiffness in AD was observed within the operculum and the precentral gyrus, both of which are located in the frontal lobe. The operculum, a deep cortical structure which forms part of the inferior frontal gyrus, has been suggested to be involved in integrating exteroceptive and interoceptive signals necessary for interoceptive awareness (Blefari *et al.*, 2017)—a deficit in which may be responsible for the lack of insight which is a frequent symptom of dementia (Tsakiris and Critchley, 2016). Functional MRI studies have also revealed decreased activation of the operculum in semantic episodic memory word paradigms in MCI participants compared with healthy controls (Jin *et al.*, 2012). Abnormal connectivity between the precentral gyrus and other brain regions has also been implicated in AD which may be related to language impairments often observed in this population. Furthermore, machine learning findings have suggested that the precentral gyrus is one of several regions affected in AD (Zhang *et al.*, 2015). Of particular interest is that volumetric differences were not detected between OA and AD in either the operculum or precentral gyrus, and the MRE effect persisted when regional volumes were controlled for. This suggests that MRE may be able to detect microstructural alterations prior to neurodegenerative effects; however, this statement cannot be inferred directly from the cross-sectional data presented here.

Interestingly, we did not find any difference in hippocampal stiffness between OA and AD despite the difference between groups in hippocampal volume. This is inconsistent with a previous study by Gerischer *et al.*, (2018) who reported a ~22% reduction in both hippocampal stiffness and volume in AD patients compared with healthy controls (Gerischer *et al.*, 2018). One potential explanation for this discrepancy may be related to the difference in ages between our two groups, with the OA group being significantly younger than the AD group. Without age correction, we would indeed see a ~11% decrease in hippocampal stiffness in AD ($P = 0.046$), although it is likely that increasing age would account for part of the decreased stiffness reported. What is evident, however, is that highly significant MRE effects are noted for regions of the cortex which have not previously been reported to be affected by AD. In addition, animal models have yet to demonstrate whether hippocampal stiffness changes are due to amyloid deposition or indicative of tau-pathology, neuronal loss or inflammatory processes, and longitudinal studies will be required to track changes to hippocampal stiffness throughout healthy or pathological aging processes.

We also did not find any significant differences in the damping ratio, ξ, either for the global or voxel-wise analysis. For completeness, we present data for ξ in Supplementary Table 2 for the same eight regions that were investigated in the *post hoc* analyses for stiffness. While our data did not reach statistical significance, we found a general trend that hippocampal ξ was lower in AD (OA: 0.201; AD: 0.177) indicating a more elastic as opposed to viscous material property. These results are consistent with both human (Gerischer *et al.*, 2018) and mouse model (Munder *et al.*, 2018) investigations that had reported a reduction in hippocampal viscosity due to AD. Apparently, somewhat contradictorily, lower ξ of the hippocampus has also been reported to be associated with better memory performance in healthy participants (Schwarb *et al.*, 2016, 2017; Hiscox *et al.*, 2018*b*). The presence of AD neuropathology, however, is likely to affect hippocampal mechanical properties differently than those that govern memory function in healthy participants. For example, a decrease in ξ in AD may be due to the structural abnormalities that define AD, such as amyloid plaque formation, which are not present in healthy tissue. Further work is needed to examine individuals at different stages of disease progression to elucidate the temporal effects of AD pathology on hippocampal ξ and their relationship to changes in cognitive functions such as memory.

AD is conceptualized as a progressive consequence of two hallmark pathological changes in GM, namely, extracellular amyloid plaques and neurofibrillary tangles, and perhaps in consequence the present study has focused on elucidating mechanical alterations to the cerebral cortex. However, previous neuroimaging studies have implicated micro- and macrostructural abnormalities in WM in the risk and progression of AD (Nasrabady *et al.*, 2018); for example, WM degeneration and demyelination may also be important pathophysiological features of the disease. We reported a significant reduction of 9% in WM stiffness in AD at the global level, which is consistent with findings from Gerischer *et al.*, (2018) who reported a 11% reduction in WM stiffness. Interestingly, evidence suggests that WM stiffness is directly proportional to local myelin content (Weickenmeier *et al.*, 2016) and that myelin not only insulates signal propagation but also provides structural support by playing an important

mechanical role. Due to current limitations of our inversion method, which is based on an isotropic material model that assumes no directional dependence of anatomical fibres, we did not analyse the mechanical properties of the WM tracts in the present study. However, preliminary work is underway to incorporate anisotropic material properties within the NLI framework for MRE (Anderson *et al.*, 2016), which in the future may reveal new insights into the mechanical properties of the WM tracts and its relationship with demyelination processes that occur in AD.

A limitation of the present study is the lack of knowledge regarding the true spatial resolution of the MRE property maps when investigating the mechanical properties of the cerebral cortex. This could raise concern regarding partial volume effects, particularly for the AD group who, although it was not the case in the present study, are expected to have a thinner cortex. Evaluations of our NLI technique using 2 mm isotropic data obtained for phantoms has led to the suggestion that within 3–5 mm of an interface partial voluming may affect the stiffness of neighbouring regions (Solamen *et al.*, 2018). Nevertheless, the authors suggest that even smaller structures with lower contrast between regions would be visible with higher-resolution acquisition data, such as the 1.6 mm isotropic data that we present in this study. Furthermore, we use *a priori* spatial information to improve the mechanical property estimates in small cortical structures (Johnson *et al.*, 2016). Based on our analysis of the effect of SPR parameters on MRE estimates (Supplementary Table 1), we find that our results remain the same despite the fact that the stiffness estimates in different regions respond more or less sensitively to regularization weightings. Regional size, geometry, mechanical interfaces and local signal to noise ratio are all likely to influence the effect of interaction of specific SPR weighting on final MRE estimates, so a direct correlation between regularization parameters and final property estimate would not be expected. Nevertheless, we cannot guarantee that higher-resolution displacement data or the use of SPR definitively overcome the effects of small structure volume on MRE property estimates, and thus, we additionally control for structure volume in statistical tests between groups. We acknowledge that using volume as a control variable is only a first-order approximation of the partial volume effects on stiffness and it is unknown if the mapping is linear, though the fact that the statistical trends remain largely unchanged provides support that the MRE measures are reliable.

There are several other limitations to this preliminary exploratory investigation. First, AD patients did not have biomarker-confirmed AD. A recent research framework has focused on AD diagnosis in living persons based on amyloid deposition, pathologic tau and neurodegeneration [AT(N)] such that diagnosis is not simply based on the clinical consequences of the disease (Jack *et al.*, 2018). In future, MRE could be applied with participants selected according to ATN criteria. Second, data regarding disease duration were not available, which may be important as this is likely to modulate the distribution of cortical involvement (Karas *et al.*, 2007). Third, we acknowledge the small sample sizes for both the AD and OA groups which limit statistical power. However, despite the small sample, we have replicated previous findings that describe a reduction in global brain stiffness in AD patients and report large effect sizes for specific regions of the cortex that may be investigated in future studies with larger sample sizes. Finally, there remains ambiguity about the neurobiological basis of the MRE signal with several different biological mechanisms having been linked to alterations in brain viscoelastic properties. More detailed comparisons between MRE, histology, microscopy and other imaging techniques will be needed to disentangle the relationship between mechanical properties and neurobiology, which is likely to change during the temporal progression of AD.

Conclusions

To the best of our knowledge, we have performed the first exploratory voxel-wise investigation to identify both volumetric and viscoelastic alterations across the cerebral cortex due to AD. We report GM volume deficits and reduced stiffness across the cortex of the temporal and parietal lobes among AD participants. Lower stiffness in AD was also identified within regions of the frontal lobe; regions that did not, however, show smaller volumes when compared with OA. A *post hoc* region of interest approach confirmed the findings from the voxel-wise analyses and suggest MRE may provide uniquely high sensitivity to AD neuropathology. Future studies in which MRE is applied in biomarker-confirmed, high-risk populations in the prodromal stages of AD are likely to be highly informative.

Supplementary material

Supplementary material is available at *Brain Communications* online.

Acknowledgements

We express our sincere thanks to all participants who took part in this study, and to all of the Radiographers at the Edinburgh Imaging Facility, QMRI. We are grateful to have been able to access the Join Dementia Research (JDR) database. JDR is funded by the Department of Health and delivered by the National Institute for Health Research in partnership with Alzheimer Scotland, Alzheimer's Research UK and Alzheimer's Society—www.joindementiaresearch.nihr.ac.uk.

Funding

L.V.H. was funded through a grant to the University of Edinburgh from Alzheimer Scotland. This research was also partially supported by the National Institute on Aging of the National Institutes of Health (R01-AG058853).

Competing interests

The authors report no competing interests.

References

Aggleton JP, Brown MW. Episodic memory, amnesia, and the hippocampal–anterior thalamic axis. Behav Brain Sci 1999; 22: 425–44.

Agosta F, Pievani M, Geroldi C, Copetti M, Frisoni G, Filippi M. Resting state fMRI in Alzheimer's disease: beyond the default mode network. Neurobiol Aging 2012; 33: 1564–8.

Alzheimer's Association. 2018. Alzheimer's disease facts and figures. Alzheimer's Dement 2018; 14: 367–429.

Anderson AT, Van Houten EEW, McGarry MDJ, Paulsen KD, Holtrop JL, Sutton BP, et al. Observation of direction-dependent mechanical properties in the human brain with multi-excitation MR elastography. J Mech Behav Biomed Mater 2016; 59: 538–46.

Arani A, Murphy M, Glaser K, Manduca A, Lake D, Kruse S, et al. Measuring the effects of aging and sex on regional brain stiffness with MR elastography in healthy older adults. Neuroimage 2015; 111: 59–64.

Ashburner J. A fast diffeomorphic image registration algorithm. Neuroimage 2007; 38: 95–113.

Bigot M, Chauveau F, Beuf O, Lambert SA. Magnetic resonance elastography of rodent brain. Front Neurol 2018; 9: 1010.

Blefari ML, Martuzzi R, Salomon R, Bello-Ruiz J, Herbelin B, Serino A, et al. Bilateral rolandic operculum processing underlying heartbeat awareness reflects changes in bodily self-consciousness. Eur J Neurosci 2017; 45: 1300–12.

Braak H, Braak E. Neuropathological stageing of Alzheimer-related changes. Acta Neuropathol 1991; 82: 239–59.

Canter RG, Penney J, Tsai LH. The road to restoring neural circuits for the treatment of Alzheimer's disease. Nature 2016; 539: 187–96.

Desikan RS, Segonne F, Fischl B, Quinn BT, Dickerson BC, Blacker D, et al. An automated labeling system for subdividing the human cerebral cortex on MRI scans into gyral based regions of interest. Neuroimage 2006; 31: 968–80.

Eichenbaum H, Yonelinas AP, Ranganath C. The medial temporal lobe and recognition memory. Annu Rev Neurosci 2007; 30: 123–52.

ElSheikh M, Arani A, Perry A, Boeve BF, Meyer FB, Savica R, et al. MR elastography demonstrates unique regional brain stiffness patterns in dementias. AJR Am J Roentgenol 2017; 209: 403–8.

European Medicines Agency. Qualification opinion of low hippocampal volume (atrophy) by MRI for use in regulatory clinical trials—in pre-dementia stage of Alzheimer's disease, 2011. Available at: http://www.ema.europa.eu/docs/en_GB/document_library/Regulatory_and_procedural_guideline/2011/12/WC500118737.pdf.

Fischl B, Salat DH, Busa E, Albert M, Dieterich M, Haselgrove C, et al. Whole brain segmentation: automated labeling of neuroanatomical structures in the human brain. Neuron 2002; 33: 341–55.

Freimann F, Muller S, Streitberger K, Guo J, Rot S, Ghori A, et al. MR elastography in a murine stroke model reveals correlation of macroscopic viscoelastic properties of the brain with neuronal density. NMR Biomed 2013; 26: 1534–9.

Frisoni G, Fox N, Jack C Jr, Scheltens P, Thompson P. The clinical use of structural MRI in Alzheimer disease. Nat Rev Neurol 2010; 6: 67–77.

Gerischer LM, Fehlner A, Köbe T, Prehn K, Antonenko D, Grittner U, et al. Combining viscoelasticity, diffusivity and volume of the hippocampus for the diagnosis of Alzheimer's disease based on magnetic resonance imaging. NeuroImage Clin 2018; 18: 485–93.

Gonneaud J, Arenaza-Urquijo EM, Mezenge F, Landeau B, Gaubert M, Bejanin A, et al. Increased florbetapir binding in the temporal neocortex from age 20 to 60 years. Neurology 2017; 89: 2438–46.

Halliday G. Pathology and hippocampal atrophy in Alzheimer's disease. Lancet Neurol 2017; 16: 862–4.

Hardy JA, Higgins GA. Alzheimer's disease: the amyloid cascade hypothesis. Science 1992; 256: 184–5.

Hiscox LV, Johnson CL, Barnhill E, McGarry MDJ, Iii Huston J, van Beek EJR, et al. Magnetic resonance elastography (MRE) of the human brain: technique, findings and clinical applications. Phys Med Biol 2016; 61: R401–37.

Hiscox LV, Johnson CL, McGarry MDJ, Perrins M, Littlejohn A, van Beek EJR, et al. High-resolution magnetic resonance elastography reveals differences in subcortical gray matter viscoelasticity between young and healthy older adults. Neurobiol Aging 2018a; 65: 158–67.

Hiscox LV, Johnson CL, McGarry MDJ, Schwarb H, van Beek EJR, Roberts N, et al. Hippocampal viscoelasticity and episodic memory performance in healthy older adults examined with magnetic resonance elastography. Brain Imaging Behav 2018b. doi: 10.1007/s11682-018-9988-8.

Jack CR, Bennett DA, Blennow K, Carrillo MC, Dunn B, Haeberlein SB, et al. NIA-AA research framework: toward a biological definition of Alzheimer's disease. Alzheimer's and Dementia 2018; 14: 535–62.

Jack CR, Lowe VJ, Senjem ML, Weigand SD, Kemp BJ, Shiung MM, et al. 11C PiB and structural MRI provide complementary information in imaging of Alzheimer's disease and amnestic mild cognitive impairment. Brain 2008; 131: 665–80.

Jack CJ, Barkhof F, Bernstein MA, Cantillon M, Cole PE, Decarli C, et al. Steps to standardization and validation of hippocampal volumetry as a biomarker in clinical trials and diagnostic criterion for Alzheimer's disease. Alzheimers Dement 2011; 7: 474–85.

Jack CJ, Reyes D, Gunter JL, Senjem ML, Vemuri P, Lowe V, et al. Different definitions of neurodegeneration produce similar amyloid/neurodegeneration biomarker group findings. Brain 2015; 138: 3747–59.

Jack CRJ, Knopman DS, Jagust WJ, Shaw LM, Aisen PS, Weiner MW, et al. Hypothetical model of dynamic biomarkers of the Alzheimer's pathological cascade. Lancet Neurol 2010; 9: 119–28.

Jenkinson M, Beckmann C, Behrens T, Woolrich M, Smith S. FSL. NeuroImage 2012; 62: 782–90.

Jin M, Pelak VS, Curran T, Nandy RR, Cordes D. A preliminary study of functional abnormalities in aMCI subjects during different episodic memory tasks. Magn Reson Imaging 2012; 30: 459–70.

Johnson CL, Holtrop JL, McGarry MDJ, Weaver JB, Paulsen KD, Georgiadis JG, et al. 3D multislab, multishot acquisition for fast, whole-brain MR elastography with high signal-to- noise efficiency. Magn Reson Med 2014; 71: 477–85.

Johnson CL, Schwarb H, Horecka KM, McGarry MDJ, Hillman CH, Kramer AF, et al. Double dissociation of structure-function relationships in memory and fluid intelligence observed with magnetic resonance elastography. Neuroimage 2018; 171: 99–106.

Johnson CL, Schwarb H, McGarry MDJ, Anderson AT, Huesmann GR, Sutton BP, et al. Viscoelasticity of subcortical gray matter structures. Hum Brain Mapp 2016; 12: 4221–33.

Karas G, Scheltens P, Rombouts S, van Schijndel R, Klein M, Jones B, et al. Precuneus atrophy in early-onset Alzheimer's disease: a morphometric structural MRI study. Neuroradiology 2007; 49: 967–76.

Klasson N, Olsson E, Eckerström C, Malmgren H, Wallin A. Estimated intracranial volume from FreeSurfer is biased by total brain volume. Eur Radiol Exp 2018; doi: 10.1186/s41747-018-0055-4.

Klein C, Hain EG, Braun J, Riek K, Mueller S, Steiner B, et al. Enhanced adult neurogenesis increases brain stiffness: in vivo magnetic resonance elastography in a mouse model of dopamine depletion. PLoS One 2014; 9: e92582.

Leech R, Sharp DJ. The role of the posterior cingulate cortex in cognition and disease. Brain 2014; 137: 12–32.

Lu Y, Franze K, Seifert G, Steinhauser C, Kirchhoff F, Wolburg H, et al. Viscoelastic properties of individual glial cells and neurons in the CNS. Proc Natl Acad Sci USA 2006; 103: 17759–64.

Maldjian JA, Laurienti PJ, Kraft RA, Burdette JH. An automated method for neuroanatomic and cytoarchitectonic atlas-based interrogation of fMRI data sets. Neuroimage 2003; 19: 1233–9.

Mariappan Y, Glaser K, Ehman R. Magnetic resonance elastography: a review. Clin Anat 2010; 23: 497–511.

McGarry M, Johnson CL, Sutton BP, Van Houten EE, Georgiadis JG, Weaver JB, et al. Including spatial information in nonlinear inversion MR elastography using soft prior regularization. IEEE Trans Med Imaging 2013; 32: 1901–9.

McGarry M, Van Houten E. Use of a Rayleigh damping model in elastography. Med Biol Eng Comput 2008; 46: 759–66.

McGarry M, Van Houten E, Johnson C, Georgiadis J, Sutton B, Weaver J, et al. Multiresolution MR elastography using nonlinear inversion. Med Phys 2012; 39: 6388–96.

McGarry M, Van Houten E, Perrinez P, Pattison A, Weaver J, Paulsen K. An octahedral shear strain-based measure of SNR for 3D MR elastography. Phys Med Biol 2011; 56: 153–64.

McRae-McKee K, Evans S, Hadjichrysanthou C, Wong MM, de Wolf F, Anderson RM. Combining hippocampal volume metrics to better understand Alzheimer's disease progression in at-risk individuals. Sci Rep 2019; 9: 7499.

Menal MJ, Jorba I, Torres M, Montserrat JM, Gozal D, Colell A, et al. Alzheimer's disease mutant mice exhibit reduced brain tissue stiffness compared to wild-type mice in both normoxia and following intermittent hypoxia mimicking sleep apnea. Front Neurol 2018; 9: 1.

Migliaccio R, Agosta F, Possin KL, Canu E, Filippi M, Rabinovici GD, et al. Mapping the progression of atrophy in early- and late-onset Alzheimer's disease. JAD 2015; 46: 351–64.

Munder T, Pfeffer A, Schreyer S, Guo J, Braun J, Sack I, et al. MR elastography detection of early viscoelastic response of the murine hippocampus to amyloid beta accumulation and neuronal cell loss due to Alzheimer's disease. J Magn Reson Imaging 2018; 47: 105–14.

Murphy MC, Curran GL, Glaser KJ, Rossman PJ, Huston J, Poduslo JF, et al. Magnetic resonance elastography of the brain in a mouse model of Alzheimer's disease: initial results. J Mag Reson Imaging 2012; 30: 535–9.

Murphy MC, Huston J, Ehman RL. MR elastography of the brain and its application in neurological diseases. NeuroImage 2019; 187: 176–83.

Murphy MC, Huston J, Jack CR, Glaser KJ, Manduca A, Felmlee JP, et al. Decreased brain stiffness in Alzheimer's disease determined by magnetic resonance elastography. J Magn Reson Imaging 2011; 34: 494–8.

Murphy M, Jones D, Jack C, Glaser K, Senjem M, Manduca A, et al. Regional brain stiffness changes across the Alzheimer's disease spectrum. Neuroimage Clin 2016; 10: 283–90.

Muthupillai R, Lomas D, Rossman P, Greenleaf J, Manduca A, Ehman R. Magnetic resonance elastography by direct visualization of propagating acoustic strain waves. Science 1995; 169: 1854–7.

Nasrabady SE, Rizvi B, Goldman JE, Brickman AM. White matter changes in Alzheimer's disease: a focus on myelin and oligodendrocytes. Acta Neuropathol Commun 2018; 6: 22.

Nasreddine ZS, Phillips NA, Bã©Dirian VÃ©R, Charbonneau S, Whitehead V, Collin I, et al. The montreal cognitive assessment, MoCA: a brief screening tool for mild cognitive impairment. J Am Geriatr Soc 2005; 53: 695–9.

Peelle JE, Cusack R, Henson R. Adjusting for global effects in voxel-based morphometry: gray matter decline in normal aging. NeuroImage 2012; 60: 1503–16.

Raz N, Lindenberger U, Rodrigue K, Kennedy K, Head D, Williamson A, et al. Regional brain changes in aging healthy adults: general trends, individual differences and modifiers. Cereb Cortex 2005; 15: 1676–89.

Riek K, Millward J, Hamann I, Mueller S, Pfueller C, Paul F, et al. Magnetic resonance elastography reveals altered brain viscoelasticity in experimental autoimmune encephalomyelitis. Neuroimage Clin 2012; 1: 81–90.

Risacher S, Saykin A. Neuroimaging biomarkers of neurodegenerative diseases and dementia. Semin Neurol 2013; 33: 386–416.

Ritchie K, Ritchie CW, Yaffe K, Skoog I, Scarmeas N. Is late-onset Alzheimer's disease really a disease of midlife? Alzheimers Dement 2015; 1: 122–30.

Rodriguez-Arellano JJ, Parpura V, Zorec R, Verkhratsky A. Astrocytes in physiological aging and Alzheimer's disease. Neuroscience 2016; 323: 170–82.

Sack I, Johrens K, Wurfel J, Braun J. Structure-sensitive elastography: on the viscoelastic powerlaw behavior of in vivo human tissue in health and disease. Soft Matter 2013; 9: 5672–80.

Schmidt P, Gaser C, Arsic M, Buck D, Förschler A, Berthele A, et al. An automated tool for detection of FLAIR-hyperintense white-matter lesions in Multiple Sclerosis. NeuroImage 2012; 59: 3774–83.

Schregel K, Wuerfel E, Garteiser P, Gemeinhardt I, Prozorovski T, Aktas O, et al. Demyelination reduces brain parenchymal stiffness quantified in vivo by magnetic resonance elastography. Proc Natl Acad Sci USA 2012; 109: 6650–5.

Schuff N, Woerner N, Boreta L, Kornfield T, Shaw LM, Trojanowski JQ, et al.; the Alzheimer's Disease Neuroimaging Initiative. MRI of hippocampal volume loss in early Alzheimer's disease in relation to ApoE genotype and biomarkers. Brain 2009; 132: 1067–77.

Schwarb H, Johnson CL, Daugherty A, Hillman C, Kramer A, Cohen N, et al. Aerobic fitness, hippocampal viscoelasticity, and relational memory performance. NeuroImage 2017; 153: 179–88.

Schwarb H, Johnson CL, Dulas MR, McGarry MDJ, Holtrop JL, Watson PD, et al. Structural and functional MRI evidence for distinct medial temporal and prefrontal roles in context-dependent relational memory. J Cogn Neurosci 2019; 31: 1857–72.

Schwarb H, Johnson CL, McGarry MDJ, Cohen N. Medial temporal lobe viscoelasticity and relational memory performance. NeuroImage 2016; 132: 534–41.

Solamen LM, McGarry MD, Tan L, Weaver JB, Paulsen KD. Phantom evaluations of nonlinear inversion MR elastography. Phys Med Biol 2018; 63: 145021.

Song Z, Insel PS, Buckley S, Yohannes S, Mezher A, Simonson A, et al. Brain amyloid- burden is associated with disruption of intrinsic functional connectivity within the medial temporal lobe in cognitively normal elderly. J Neurosci 2015; 35: 3240–7.

Spenger C, Eskildsen S, Sjogren N, Julin P, Westman E, Wahlund LO, et al. Cortical atrophy rates in Alzheimer's disease and mild cognitive impairment from the ADNI study. Alzheimers Dement 2011; 7: S225.

Tsakiris M, Critchley H. Interoception beyond homeostasis: affect, cognition and mental health. Phil Trans R Soc B 2016; 371: 20160002.

Tzourio-Mazoyer N, Landeau B, Papathanassiou D, Crivello F, Etard O, Delcroix N, et al. Automated anatomical labeling of activations in SPM using a macroscopic anatomical parcellation of the MNI MRI single-subject brain. Neuroimage 2002; 15: 273–89.

Utevsky AV, Smith DV, Huettel SA. Precuneus is a functional core of the default-mode network. J Neurosci 2014; 34: 932–40.

Van Houten E, Paulsen K, Miga M, Kennedy F, Weaver J. An overlapping subzone technique for MR-based elastic property reconstruction. Magn Reson Med 1999; 42: 779–86.

Weickenmeier J, de Rooij R, Budday S, Ovaert TC, Kuhl E. The mechanical importance of myelination in the central nervous system. J Mech Behav Biomed Mater 2017; 76: 119–24.

Weickenmeier J, de Rooij R, Budday S, Steinmann P, Ovaert TC, Kuhl E. Brain stiffness increases with myelin content. Acta Biomater 2016; 42: 265–72.

Zhang Y, Dong Z, Phillips P, Wang S, Ji G, Yang J, et al. Detection of subjects and brain regions related to Alzheimer's disease using 3DMRI scans based on eigenbrain and machine learning. Front Comput Neurosci 2015. doi: 10.3389/fncom.2015.00066.